UC Irvine
UC Irvine Previously Published Works

Title

Differential modulation of the molecular dynamics of the type IIa and IIc sodium phosphate cotransporters by parathyroid hormone

Permalink

https://escholarship.org/uc/item/1sq4p8qv

Journal

American Journal of Physiology - Cell Physiology, 301(4)

ISSN

0363-6143

Authors

Lanzano, Luca
Lei, Tim
Okamura, Kayo
et al.

Publication Date

2011-10-01

DOI

10.1152/ajpcell.00412.2010

Copyright Information

Peer reviewed

Differential modulation of the molecular dynamics of the type IIa and IIc sodium phosphate cotransporters by parathyroid hormone

Luca Lanzano,[1]* Tim Lei,[3]* Kayo Okamura,[2]* Hector Giral,[2] Yupanqui Caldas,[2] Omid Masihzadeh,[3] Enrico Gratton,[1] Moshe Levi,[2,4] and Judith Blaine[2]

[1]*Laboratory for Fluorescence Dynamics, University of California, Irvine, California; and Departments of* [2]*Medicine,* [3]*Electrical Engineering, and* [4]*Physiology and Biophysics, University of Colorado, Aurora, Colorado*

Lanzano L, Lei T, Okamura K, Giral H, Caldas Y, Masihzadeh O, Gratton E, Levi M, Blaine J. Differential modulation of the molecular dynamics of the type IIa and IIc sodium phosphate cotransporters by parathyroid hormone. *Am J Physiol Cell Physiol* 301: C850–C861, 2011. First published May 18, 2011; doi:10.1152/ajpcell.00412.2010.—The kidney is a key regulator of phosphate homeostasis. There are two predominant renal sodium phosphate cotransporters, NaPi2a and NaPi2c. Both are regulated by parathyroid hormone (PTH), which decreases the abundance of the NaPi cotransporters in the apical membrane of renal proximal tubule cells. The time course of PTH-induced removal of the two cotransporters from the apical membrane, however, is markedly different for NaPi2a compared with NaPi2c. In animals and in cell culture, PTH treatment results in almost complete removal of NaPi2a from the brush border (BB) within 1 h whereas for NaPi2c this process in not complete until 4 to 8 h after PTH treatment. The reason for this is poorly understood. We have previously shown that the unconventional myosin motor myosin VI is required for PTH-induced removal of NaPi2a from the proximal tubule BB. Here we demonstrate that myosin VI is also necessary for PTH-induced removal of NaPi2c from the apical membrane. In addition, we show that, while at baseline the two cotransporters have similar diffusion coefficients within the membrane, after PTH addition the diffusion coefficient for NaPi2a initially exceeds that for NaPi2c. Thus NaPi2c appears to remain "tethered" in the apical membrane for longer periods of time after PTH treatment, accounting, at least in part, for the difference in response times to PTH of NaPi2a versus NaPi2c.

apical trafficking; myosin VI

PHOSPHATE HOMEOSTASIS IS CRUCIAL for many important cellular processes including energy production, cell signaling, and bone formation (13). The kidney plays a critical role in the regulation of phosphate balance. At physiologic pH, the majority of the renal handling of phosphorous occurs via two sodium phosphate cotransporters, NaPi2a and NaPi2c, with a third sodium phosphate cotransporter known as Pit-2 playing a much lesser role (41). All three sodium phosphate cotransporters are expressed in the apical brush border (BB) membrane of renal proximal tubule cells (23).

Parathyroid hormone (PTH) is a key element in the maintenance of phosphorous balance. PTH acts to decrease the abundance of NaPi2a and NaPi2c in the proximal tubule BB. The brush border membrane (BBM) consists of hundreds of densely packed microvilli which increase the absorptive surface of proximal tubule cells. Each microvillus contains a central actin bundle arrayed so that the plus end is pointing toward the luminal surface (4). The actin core undergoes a process known as treadmilling, in which actin monomers come off the minus end and are added to the plus end (6, 35). At steady state this process is in balance so that the actin bundle remains constant in length (6).

In addition to actin, the microvillus also contains scaffolding or PDZ proteins (18, 23, 30). The PDZ protein sodium-hydrogen exchanger regulatory factor-1 (NHERF-1) has been shown to be critical for PTH-induced trafficking of NaPi2a (8, 10, 20, 28). In addition, NaPi2a has also been shown to interact with NHERF-3 (PDZK1) (27, 31). NaPi2c has also been shown to interact with NHERF-1 and NHERF-3 (27, 39). However, the precise mechanistic details of how NaPi2c/PDZ protein interactions are altered by PTH remain to be determined.

Myosin VI is an unconventional motor protein that is also found in the microvillus (44, 45). In contrast to other known myosin motor proteins, myosin VI walks toward the minus end of actin, making it an ideal candidate to pull cargo out of the microvillus. We have previously shown that myosin VI is required for PTH-induced removal of NaPi2a from the BBM (3). Here we investigate whether myosin VI is needed for PTH-induced removal of NaPi2c from BB microvilli. In addition, we examine how the diffusion coefficients of the two cotransporters change after addition of PTH.

EXPERIMENTAL PROCEDURES

Animals. C57/BL6 mice weighing between 20 and 25 g were obtained from Jackson Laboratory (Bar Harbor, MA) at the age of 6 wk. All experiments were performed in mice between the ages of 9 and 12 wk. Mice were housed in the animal facility at the University of Colorado Denver. All animal work was approved by the Institutional Animal Care and Use Committee of the University of Colorado Denver. Before euthanasia, mice were injected via tail vein with 20 μg PTH 1-34/100 g body wt.

Cell culture. Opossum kidney (OK) proximal tubule (OKP) cells that are responsive to PTH were a gift from Dr. J. Cole (University of Memphis, Memphis, TN) and were grown in DMEM/F-12 (Invitrogen, Carlsbad, CA) supplemented with 10% FBS, 50 U/ml penicillin and 50 μg/ml streptomycin. For total internal reflection fluorescence (TIRF) experimental work, cells were seeded on porous membrane inserts (Corning, Corning, NY). At 90% confluency, cells were transfected overnight using Lipofectamine 2000 (Invitrogen) according to the instructions provided by the manufacturer. The next day the cells were placed in DMEM/F-12 supplemented with 0.2% FBS to synchronize the cells.

Isolation of BBM from mice. BBM were isolated from mice as previously described (5). Briefly, mice were anesthetized and the renal vessels were clamped. The kidneys were removed and sliced. The entire kidneys from two mice were combined in isolation buffer (15 mM Tris·HCl, pH 7.4, 300 mM mannitol, 5 mM EGTA, and 1 Roche Complete protease inhibitor tablet per 250 ml buffer) and homogenized. BBM were prepared by double Mg^{2+} precipitation. For the first Mg^{2+} precipitation, Mg^{2+} was added to a final concentration of 15

* L. Lanzano, T. Lei, and K. Okamura contributed equally to this work.

Address for reprint requests and other correspondence: J. Blaine, Dept. of Medicine, Univ. of Colorado, 12700 E 19th Ave., C281, Aurora, CO 80045 (e-mail: Judith.Blaine@ucdenver.edu).

mM and the suspension was vortexed and shaken on ice every 5 min for 20 min before centrifugation at 2,500 g for 15 min. After a second Mg^{2+} precipitation, BBM were recovered by centrifugation at 38,000 g for 40 min. BBM were resuspended in isolation buffer and the protein content was determined by the bicinchoninic acid (BCA) assay (Pierce, Rockford, IL).

Isolation of BBM from OKP cells. OKP cells were grown to confluence in 60-mm dishes in DMEM/F-12 supplemented with 10% FBS, 50 U/ml penicillin and 50 μg/ml streptomycin. Before PTH treatment, cells were placed in DMEM/F-12 supplemented with 0.2% FBS to synchronize the cells. After treatment with PTH or vehicle the cells were rinsed twice with ice-cold PBS and scraped into isolation buffer (15 mM Tris·HCl, pH 7.4, 300 mM mannitol, 5 mM EGTA, and 1 Roche Complete protease inhibitor tablet per 250 ml buffer). Cells were homogenized by passage through a 23-gauge needle 30 times and then $MgCl_2$ was added to a final concentration of 15 mM. The cells were shaken every 5 min for a total of 20 min on ice and then centrifuged at 2,500 g for 15 min at 4°C. The supernatant was collected and centrifuged at 60,000 rpm for 40 min. The final pellet was resuspended in isolation buffer and the protein content was determined by the BCA assay. This protocol resulted in a 5-fold enrichment in the activity of maltase (an apical enzyme) compared with homogenate and a 10-fold de-enrichment in the activity of Na-K-ATPase (a basolateral enzyme).

Plasmid constructs. The green fluorescent protein (GFP)-NaPi2a plasmid was a gift from Dr. Heini Mürer (University of Zürich, Zurich, Switzerland). Yellow fluorescent protein (YFP)-NaPi2a was generated by cutting NaPi2a from this plasmid using *Bgl*II and *Sac*II and inserting it into a similarly digested EYFP-C1 plasmid (Clontech, Mountain View, CA). GFP-tagged myosin VI tail construct was a gift from Dr. T. Hasson (University of California San Diego, La Jolla, CA). Cyan fluorescent protein (CFP)-tagged myosin VI tail was generated by cutting the myosin VI tail fragment from the GFP plasmid using *Kpn*I and *Bam*HI and ligating it into a similarly digested pAmCyan1-C1 vector from Clontech. The YFP-NaPi2c clone was a kind gift of Victor Sorribas (University of Zaragoza, Zaragoza, Spain). The mCherry-tagged NaPi2c was created by subcloning NaPi2c into the pmCherry-C1 vector from Clontech.

Apical TIRF. Apical TIRF was performed as previously described (3). Briefly, OKP cells were grown to confluence on 12-mm, 0.4-μm membrane inserts (Corning, Lowell, MA). Membranes with confluent transfected cell layers were cut out of the plastic support and placed apical face down in a dish with a coverslip bottom (no. 1.5, MatTek, Ashland, MA) that contained 2 ml of the appropriate cell culture medium prewarmed to 37°C. To bring the apical cell surface into TIRF, a glass weight consisting of a tissue culture ring 8 mm in diameter (BiOptechs, Butler, PA) was placed on top of the membrane. Samples were observed using a Zeiss TIRF microscope equipped with a ×100 1.45 numerical aperture (NA) objective under the control of AxioVision software (version 4.5, Carl Zeiss, Thornwood, NJ). Laser excitation was derived from a multiline argon ion laser run at the same current setting for all experiments. The power at the sample was controlled by a neutral density filter wheel. Excitation and emission wavelengths were selected using filter set for YFP (514 nm). The laser was aligned per the manufacturer's instructions to achieve TIRF illumination. Images were taken using a Zeiss Axiocam MRm camera operating with 2 by 2 binning or a Photometrix QuantEM without binning. Oxygen was provided by the ambient air which was supplemented by 5% CO_2 and warmed to 37°C in an environmental chamber surrounding the specimen. Images were taken every 30 min. In some experiments, 200-nm fluorescent beads (Molecular Probes, Carlsbad, CA) were used as markers for the bottom of the dish. These beads can be seen in some images (e.g., Fig, 6*A*).

Confocal microscopy. Confocal images were acquired using a Zeiss 510 laser scanning confocal microscope. Enhanced YFP (eYFP)-NaPi2a or eYFP-NaPi2c were excited using a 488-nm laser. While it was not possible to exactly match the laser power and image exposure time, we did reproduce the *z*-stack and interimage delay protocols to that of the appropriate TIRF experiment.

PTH-induced internalization of NaPi2a and NaPi2c in OKP cells. A stock solution of 10^{-4} M 1–34 PTH (Bachem, King of Prussia, PA) was prepared as described (26) and stored in small aliquots at −20°C until needed. We used a saturating PTH concentration to minimize variations due to differing PTH receptor-ligand binding from cell to cell. Observational photobleaching was minimized by keeping the laser intensity low (5% or less of maximum laser power) and the exposure times short (50 ms). Because the PTH-induced removal of NaPi2c from the BBM takes place relatively slowly, to minimize photobleaching, a series of images were collected at 30-min intervals for up to 6 h. We started data acquisition immediately a suitable cell had been located in TIRF, while the sample was still settling in Z. To ensure that a focused image was always captured, we acquired an image stack consisting of 7 to 8 planes at 250-nm intervals. This minimizes the total exposure of the sample compared with manual refocusing. The plane of best focus was chosen for subsequent analysis. Movement in the *z* direction usually occurred within the first 10 to 15 min of placing the sample inside the environmental chamber on the microscope, and thereafter the plane of focus generally remained constant.

Jasplakinolide treatment. Jasplakinolide is a cell-permeable cyclic peptide that stabilizes actin filaments (7). A stock solution of 1 mM jasplakinolide (Alexis Biochemicals, San Diego, CA) in DMSO was prepared and stored at −20°C in 10-μl aliquots until needed. This stock was diluted in medium containing 0.2% FBS to a final concentration of 1 μM. The DMSO content was 0.1%. While the membranes were still mounted in their 12-well plate, cells were washed once with this medium and then 1 ml was added to the basal compartment and 0.5 ml was added to the apical compartment. This was then placed back in the incubator for 30 min. At the end of this period, cells were washed four times in DMEM containing 0.2% FBS and prepared as above for imaging.

Western blot analysis. Cell lysates (20 μg total protein) were separated by 10% SDS-PAGE (Criterion, Bio-Rad, Hercules, CA) and transferred onto nitrocellulose membranes (Bio-Rad). Membranes were blocked for 30 min at room temperature with 5% milk in PBST buffer (phosphate-buffered saline, 0.5% Tween, pH 7.4) before incubation with the primary antibody diluted in PBST-milk overnight at 4°C. The NaPi4 antibody was a kind gift of Dr. Syed Khundmiri (University of Louisville, Louisville, KY) and was used at 1:1,000. The NaPi2a and NaPi2c antibodies were produced by Davids Antibodies (Davids Biotechnologie, Regensburg, Germany) as previously described (40) and used at 1:1,000. Band intensities were normalized to the intensity of β-actin. The β-actin antibody was obtained from Sigma and used at 1:5,000. After four washes with PBST, membranes were incubated with horseradish peroxidase (HRP)-conjugated goat secondary antibodies (Pierce) for 1 h at room temperature. HRP was detected following 5 min of incubation in Supersignal West Pico Chemiluminescent Substrate or Supersignal West Dura Extended Duration Substrate (Pierce), using a charge-coupled device imaging system. Band intensities were quantified using Quantity One software.

Fluorescence correlation spectroscopy. Fluorescence correlation spectroscopy (FCS) measurements in cell culture were accomplished using the Olympus Fluoview 1000 confocal microscope. The microscope is equipped with an incubator chamber to maintain 37°C and 5% CO_2 concentration. The radial diameter of the FCS measurement spot size was calibrated to be between 180 and 200 nm. The ratio of the axial diameter to the radial diameter was assumed to be 5-to-1 due to confocal confinement. The fluorescent signal was collected by a 1.2-NA water immersion objective (Olympus UplanSApo ×60) and the fluorescence signal was split by a dichroic mirror at 560 nm. A 515/30 nm and a 620/60 nm emission filters (Chroma Technology Corp, Rockingham, VT) were used to filter the fluorescence signals for GFP and mCherry, respectively, to minimize signal bleed-through. The two photomultiplier tubes were equipped with electronics con-

figured to perform analog single photon counting for FCS measurements. The FCS sampling frequency was 100 KHz and the total sampling time was ~3 min. The acquired FCS data were analyzed with SimFCS software (www.lfd.uci.edu) developed by author E. Gratton at the University of California, Irvine. The diffusion coefficients of the labeled proteins and the fluorescence cross-correlation functions were further fitted by SimFCS.

Tracking raster image correlation spectroscopy. OKP cells were cotransfected with Cerulean-NaPi2a and mCherry-NaPi2c. Measurements of diffusion coefficients of NaPi2a and NaPi2c within the same microvillus were obtained using a novel technique which is a combination of single particle tracking (SPT) and raster image correlation spectroscopy (RICS) (19). The tracking-RICS experiments were performed using a home-built microscope at the Laboratory for Fluorescence Dynamics, whose technical details have been already described (24). A Chameleon Ultra II laser (Coherent, CA) tuned at 940 nm was used for simultaneous two-photon excitation of the Cerulean and the mCherry constructs. The fluorescence emission was collected by a 1.2-NA water immersion objective (Olympus UplanSApo ×60) and detected in the ranges 460–500 nm and 575–645 nm for channels 1 and 2, respectively.

A schematic of the tracking-RICS experiment is shown in Fig. 1. We initially identify candidate microvilli using conventional three-dimensional (3D) stack or modulation tracking imaging so that we can ascertain that the microvillus is not folded over or bent. Once a suitable microvillus is identified a raster scan is performed. Figure 1, *A* and *B*, shows a raster scan image of BB microvilli in an OK cell transiently expressing Cerulean-NaPi2a and mCherry-NaPi2c. The images are the average of an acquisition of 10 frames in both channels. Since the image is acquired on a plane (*xy*) which is transverse to the main axis (*z*) of the microvilli, the microvilli appear in section as circular spots. The size of these spots is larger than the real size of microvilli because of the combined effect of broadening due to the microscope point spread function (PSF, ~300 nm) and broadening due to the movement of the microvilli during the acquisition time. Some of the microvilli appear as isolated bright spots in both channels. We pick up one of the isolated microvilli such as the one indicated by the arrow. We point the scanner on the microvillus to track and then perform the tracking by scanning the laser spot in a circular orbit around the microvillus (Fig. 1*C*). The drawing in Fig. 1*C* shows the typical dimensions of the microvillus (width ≈ 100 nm), of the scanned orbit (orbit radius = 160 nm), and of the PSF waist (≈300 nm). Once the microvillus position is tracked at a given section, we can scan along the *z* to obtain a 3D image of the surface in the two channels (Fig. 1*D*) or keep the z constant (Fig. 1*E*) to perform the RICS measurement (Fig. 1, *F* and *G*) (19).

To keep the microvillus always at the center of the orbit we use a SPT algorithm originally developed to track the motion of particles within cells (25) and recently extended to the tracking of entire cell structures like microvilli. The orbit period is typically set to 8 ms and the position of the center of the scanning orbit is updated every 64 ms, which is fast enough to follow the movement of the microvillus. Using

Fig. 1. Schematic of the tracking-raster image correlation spectroscopy (RICS) experiment. *A* and *B*: brush border membrane (BBM) of an opossum kidney (OK) cell expressing Cerulean-NaPi2a and mCherry-NaPi2c, respectively (scale bar, 3 μm). The white arrow indicates an isolated bright spot interpreted as a microvillus and selected for tracking. *A* is the image obtained in channel 1 (NaPi2a) and *B* is the image obtained in channel 2 (NaPi2c) *C*: the point spread function (PSF) was scanned in an orbit of radius *R* around a microvillus section to detect the fluorescence intensity along the membrane. The yellow dot and arrow indicate the starting point and the direction of scanning. *D*: three-dimensional image of a microvillus obtained with the modulation tracking method [channel 1 (ch1): NaPi2a; channel 2 (ch2): NaPi2c; the *z* decreases toward the base of the microvillus; scale bar, 200 nm]. The image is color coded for intensity with red/yellow indicating regions of highest expression of NaPi2a or NaPi2c. *E*: trajectory of the microvillus in the *xy* plane obtained at fixed *z*. The black trace indicates movement in the *x*-axis and the red trace indicates movement in the *y*-axis. *F*: intensity along the orbit as a function of time for the two channels. *G*: RICS autocorrelation function extracted from each channel intensity carpet.
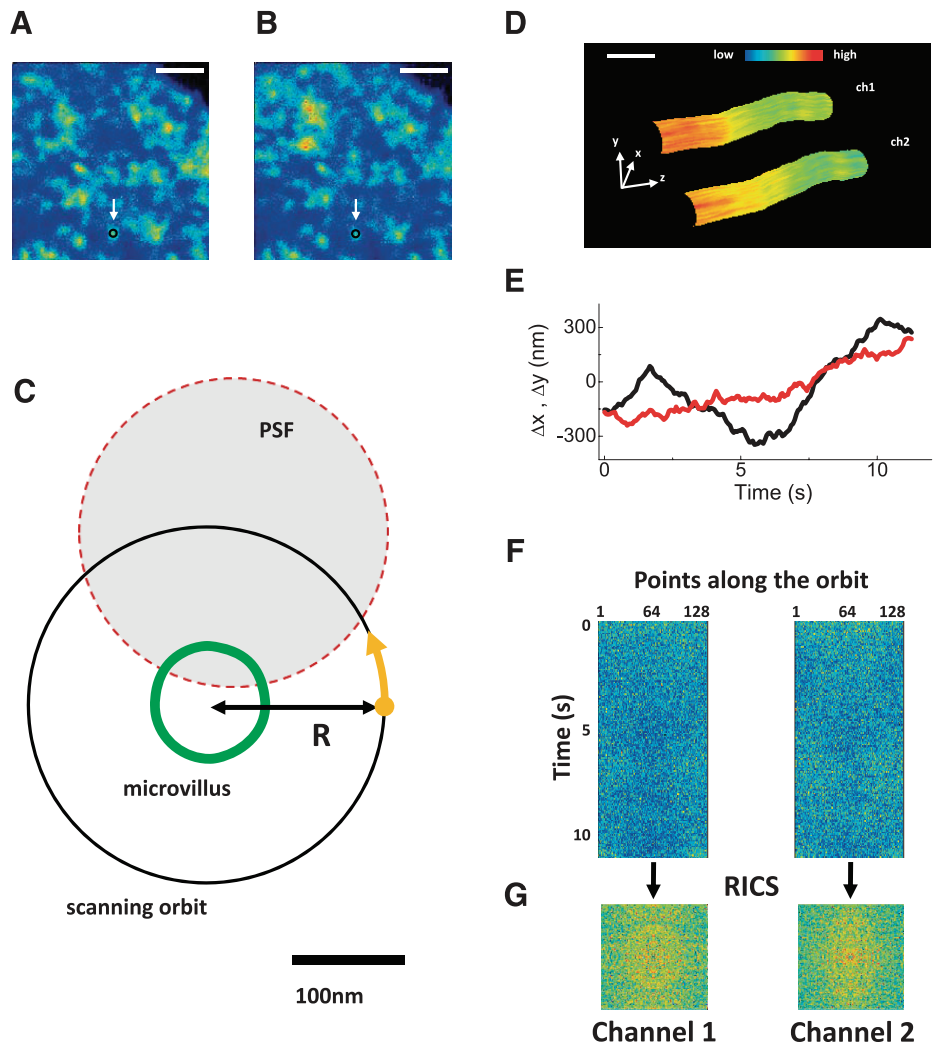
the modulation tracking method described in Ref. 19, it is possible to obtain 3D reconstructions of the microvilli surface (Fig. 1*D*) when we scan also the *z*-axis. The reconstruction is painted in color scale according to the fluorescence intensity recorded in the two channels. The size of these reconstructions is compatible with the size of single microvilli.

To perform the tracking-RICS measurement, we keep the focus fixed at a given *z* while we track the movement of the microvillus in the *xy* plane and record its trajectory (Fig. 1*E*). The fluorescence intensity is collected for both channels at 128 points along the orbit and reported in two-dimensional (2D) carpets (Fig. 1*F*) as a function of the points along the orbit (horizontal axis) and time (vertical axis). This is equivalent to scanning a line along the microvillus membrane. Since the membrane is stationary with respect to the scanned orbit, we

can analyze the fluorescence intensity fluctuations in the carpet due to diffusion of proteins along the membrane.

In line-scanning FCS the fluctuation information is contained in both temporal and spatial correlation functions that can be analyzed using the RICS technique (11, 12). We apply the RICS algorithm to the carpet to extract the temporal correlation between points on different lines (vertical axis of the carpet) and the spatial correlation between points along the same line (horizontal axis). The mathematical details of the RICS technique applied to line scanning can be found in other publications (11). We processed the data via the SimFCS software (www.lfd.uci.edu/globals) using the RICS algorithm applied to circular line-scanning data. For each intensity carpet we obtain a 2D RICS spatiotemporal autocorrelation function (Fig. 1*G*). One advantage of line-scanning RICS with respect to single-
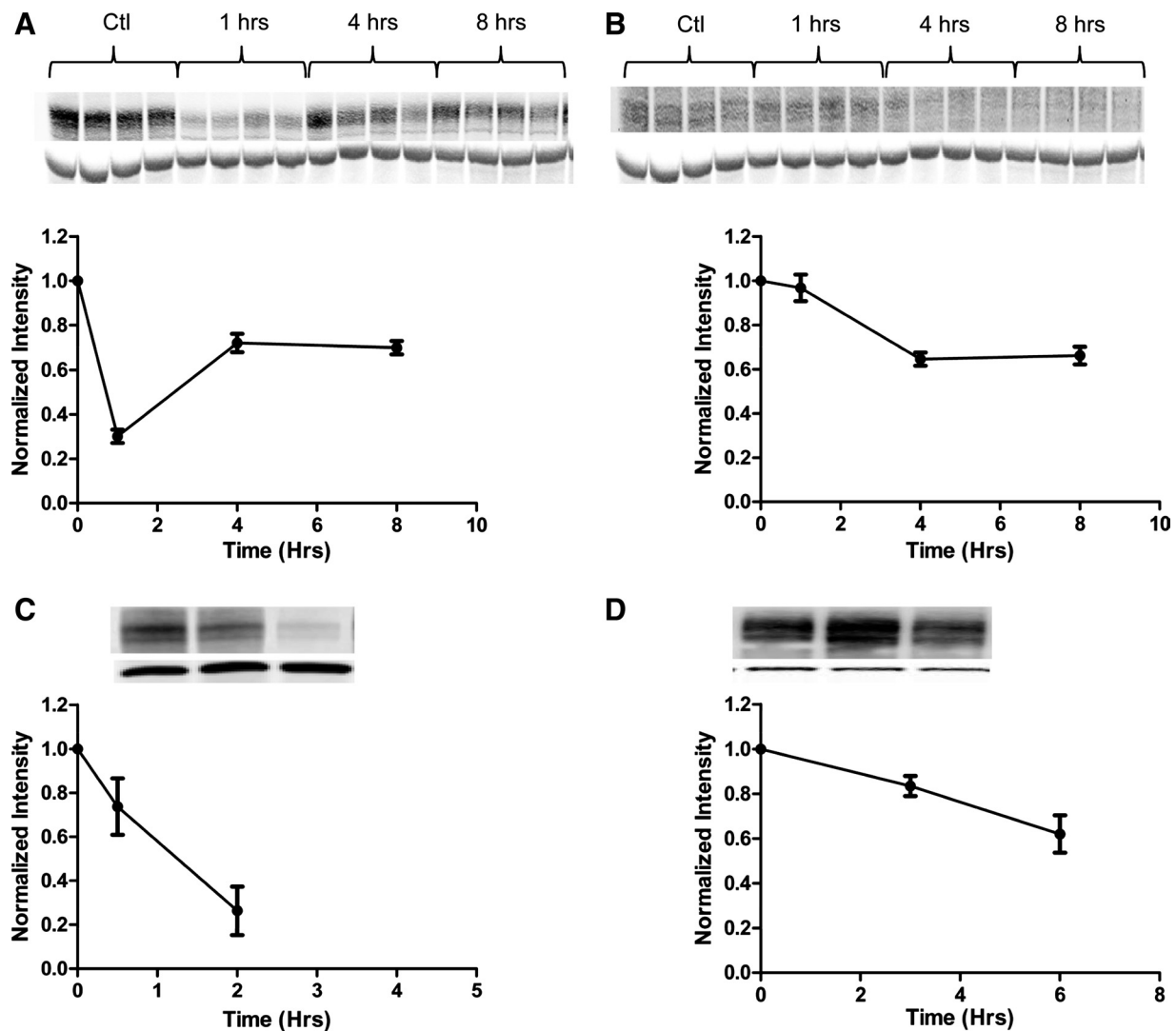

Fig. 2. Parathyroid hormone (PTH) has a differential effect on the time course of removal of NaPi2a and NaPi2c from the BBM. *A*: Western blot analysis of the brush border abundance of NaPi2a after treatment with PTH. Mice were injected with 20 μg PTH 1-34/100 g body wt or vehicle at time (*t*) = 0, and kidneys were harvested at the time points indicated. Eight animals per time point were used. Western blots are shown of 4 representative animals, and staining for actin is shown below the corresponding band of interest. To compare intensities across time points, after normalization to β-actin, all band intensities were normalized to *t* = 0. Ctl, control. Data are shown as means ± SE. *B*: Western blot analysis of the BBM abundance of NaPi2c after treatment with PTH. *C*: Western blot analysis of the brush border abundance of NaPi4 (the OK homolog to NaPi2a) in opossum kidney proximal tubule cells (OKP). Cells were treated with PTH at *t* = 0, and BBM were prepared at the time points indicated. All experiments were performed in triplicate. *D*: Western blot analysis of the brush border abundance of NaPi2c in OKP cells after treatment with PTH. OKP cells were transfected with enhanced yellow fluorescent protein (eYFP)-tagged NaPi2c and treated with PTH 48 h after transfection. Cells were harvested at the time points indicated. To account for slight differences in transfection efficiencies between dishes, the brush border abundance of eYFP-NaPi2c in each dish was normalized to the abundance of eYFP-NaPi2c in the cellular homogenate (see Supplemental Fig. S1; Supplemental Material for this article is available online at the Journal website). All experiments were performed in triplicate.

point FCS is that of being sensitive to anisotropies of molecular diffusion. Although we can detect diffusion anisotropies using this method, our data are best fit to a model of isotropic diffusion. The PSF of the instrument was calibrated using 20-nm beads fixed on a slide. The values of the diffusion coefficients were extracted fitting the results to a model of 2D diffusion.

Data analysis (statistics). For analysis of TIRF microscopy images, the average intensity of a selected region of interest (ROI) was obtained at each time point in Axiovision software (version 4.6) and corrected by the intensity measured in an ROI outside of the cell. Intensities were normalized to the initial value and plotted in Graph-Pad Prism 5 (GraphPad Software). A linear fit was applied to the data
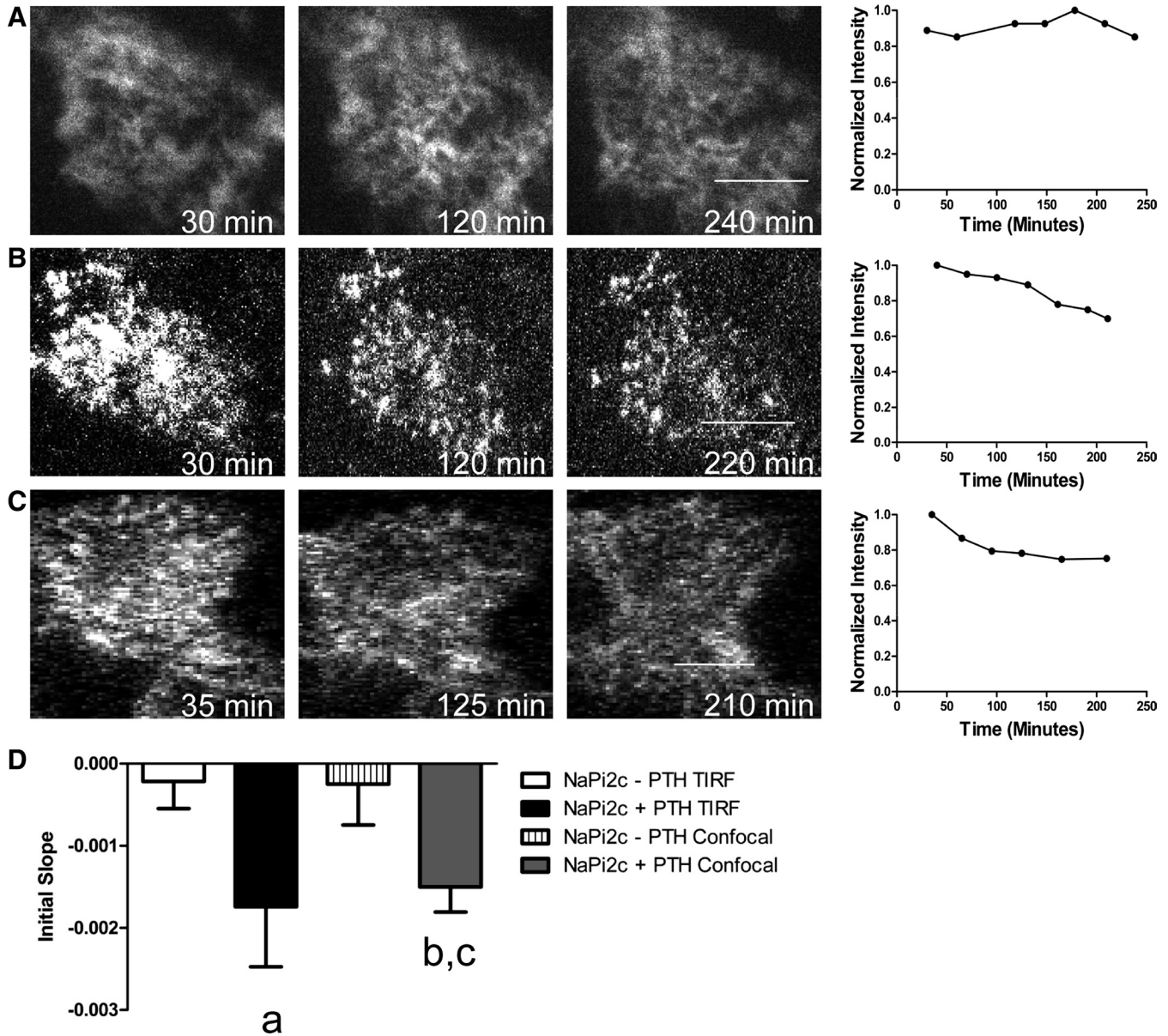

Fig. 3. Time course of PTH-induced removal of NaPi2c from the BBM as visualized by apical total internal reflection fluorescence (TIRF) microscopy (TIR-FM) and confirmed by confocal microscopy. *A*: representative image of an OKP cell transfected with eYFP-NaPi2c and not treated with PTH and imaged using TIR-FM. The graph to the *right* of the images shows changes in the fluorescence intensity over time for that cell. Fluorescence intensities were normalized to $t = 0$. A decrease in fluorescence intensity implies removal of NaPi2c from the BBM. *B*: representative image and graph of change in apical fluorescence over time of an OKP cell transfected with eYFP-NaPi2c and treated with 10^{-6} M PTH and imaged using TIR-FM. *C*: representative image and graph of change in brush border fluorescence over time of an OKP cell transfected with eYFP-NaPi2c and imaged using confocal microscopy. The results are similar to those obtained using apical TIR-FM. *D*: to compare changes in brush border fluorescence intensity over time across different cells, the slope of the intensity versus time graph for each cell was measured over the first 180 min (initial slope). A more negative slope indicates more rapid removal of NaPi2c from the BBM, while a number close to zero indicates little net turnover of the protein at the apical membrane. The bar graphs represent the average initial slopes for OKP cells transfected with eYFP-NaPi2c and not treated with PTH and imaged using TIR-FM (open bar, $n = 12$), treated with PTH and imaged using TIR-FM (black bar, $n = 18$), not treated with PTH and imaged using confocal microscopy (vertical hatched bar, $n = 7$), or treated with PTH and images using confocal microscopy (gray bar, $n = 7$). The average initial slope for cells treated with PTH and imaged using TIR-FM is significantly more negative than for untreated cells ([a]$P = 0.0104$ compared with NaPi2c − PTH). The average initial slope for cells treated with PTH and imaged using confocal microscopy is also significantly more negative ([b]$P < 0.05$ compared with NaPi2c − PTH). There is no significant difference in the initial slope for cells treated with PTH and imaged using confocal microscopy compared with TIR-FM [[c]P = not significant (NS) compared with YFP NaPi2c + PTH TIRF]. Scale bars, 5 μm.

points obtained in the first 180 min after PTH addition to obtain the rates of internalization. Statistical analysis (*t*-test for single comparisons or one-way ANOVA for multiple comparisons) was performed using GraphPad Prism 5. A *P* value < 0.05 was considered statistically significant. The *n* values given in the figure legends refer to the number of different cells analyzed for each condition.

RESULTS

PTH-induced removal of NaPi2a from the proximal tubule brush border is faster for NaPi2a than NaPi2c. Western blot analysis of BB abundance of NaPi2a or NaPi2c shows that, after treatment with PTH, removal of NaPi2a from the BBM in vivo occurs faster for NaPi2a versus NaPi2c (Fig. 2, *A* vs. *B*). The greatest decrease in BB abundance of NaPi2a occurs after 1 h, whereas for NaPi2c the same process takes 4 h.

To investigate the mechanisms underlying the difference in response to PTH for NaPi2a versus NaPi2c, we used a well-established model of the renal proximal tubule. OKP cells are derived from the opossum kidney proximal tubule and maintain their responsiveness to PTH in culture (3, 17). OKP cells endogenously express NaPi4 which is the opossum homolog to NaPi2a (21). The OKP lines in our lab, however, do not express NaPi2c (as determined by both reverse transcriptase polymerase chain reaction and immunofluorescence, data not shown). Several attempts to establish an OKP cell line that stably expresses fluorophore-tagged NaPi2c failed. To examine the effects of PTH on NaPi2c in OKP cells in culture, cells were transiently transfected with eYFP-tagged NaPi2c and then treated with PTH. Compared with NaPi4, eYFP-tagged NaPi2c shows a much slower decline in BB abundance in response to PTH (Fig. 2, *C* vs. *D*). This recapitulates what is seen in vivo.

Apical TIR-FM can be used to study the effects of PTH on the BB abundance of NaPi2c. We have previously described a novel application of TIR-FM to the apical membrane for following events at the apical surface (3). The advantage to apical TIRF compared with conventional confocal microscopy is that with apical TIRF one is certain that only events within 100 nm of the coverslip are being studied (i.e., the BBM), whereas with confocal microscopy the plane of focus can vary over time. In the previous study we also confirmed

(using confocal microscopy) that the apical TIRF method that we use does not result in any differences in cell morphology or in the time course of OKP response to PTH.

Using apical TIR-FM we studied the effects of PTH on the BB abundance of NaPi2c. OKP cells were transfected with eYFP-NaPi2c and then treated with 10^{-6} M PTH. After PTH treatment, there is a gradual reduction in BB fluorescence intensity compared with controls (Fig. 3*B*), implying removal of eYFP-NaPi2c from the microvilli. The effect can be quantified by measuring the change in slope over the first 3 h after PTH treatment (initial slope). As can be seen in Fig. 3*D*, the initial slope for eYFP-NaPi2c-transfected cells treated with PTH is significantly more negative than that for controls, implying faster removal of NaPi2c from the apical surface in cells treated with PTH ($P = 0.0104$ for initial slope of NaPi2c − PTH vs. NaPi2c + PTH). To confirm these results, OKP cells were also transfected with eYFP-NaPi2c, treated with PTH, and then imaged using confocal microscopy. As can be seen in Fig. 3, *C* and *D*, PTH treatment results in a gradual decrease in the brush border fluorescence intensity over time, results that are very similar to those obtained using apical TIR-FM. Indeed, there is no significant difference in the initial slope for cells treated with PTH and imaged using either apical TIR-FM or confocal microscopy. The disadvantage to using confocal microscopy is that it is much more difficult to ensure that one is following the same position within the apical membrane over time as the focal plane tends to drift. This becomes even more relevant when monitoring slow processes that occur over hours.

A dynamic actin cytoskeleton is required for PTH-induced trafficking of NaPi2c. Brush border microvilli contain a central actin core oriented so that the plus end is at the apical end of the microvillus and the minus end is closest to the cell interior (4) (Fig. 4 *A* and *B*). The actin core undergoes constant turnover known as treadmilling with actin monomers coming off the minus end and being added to the plus end (6, 35, 38). We have previously shown that the unconventional myosin motor myosin VI is required for PTH-induced removal of NaPi2a from the proximal tubule BB (3). One hypothesis to explain the kinetic difference in response to PTH is that NaPi2a "motors" down the microvillus using myosin VI, whereas
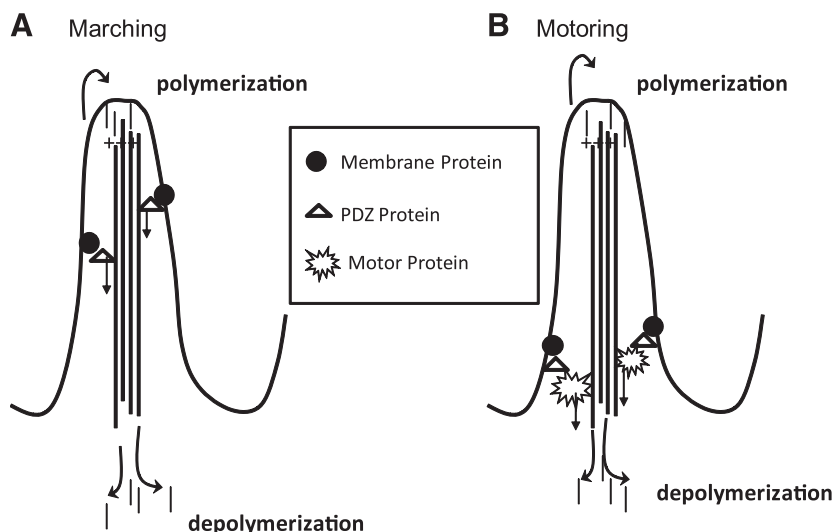

Fig. 4. Model of mechanisms for removing membrane proteins from brush border microvilli. *A*: in the "marching model," the membrane proteins are linked directly to the central actin core in the microvillus via PDZ proteins and are removed from the microvillus via treadmilling of the actin core. *B*: in the "motoring" model, the membrane proteins are linked to a myosin motor and are moved out of the microvillus by the actions of the motor protein. Motoring as a means of removal of proteins from the microvillus would be expected to be more rapid than marching.

NaPi2c is directly attached to the actin core and is moved out of the microvillus by treadmilling (Fig. 4, *A* and *B*). Treadmilling or "motoring" as a means of removal of NaPi2c from the BBM would both require a dynamic actin cytoskeleton. To examine whether a dynamic actin cytoskeleton is required for PTH-induced removal of NaPi2c from BB microvilli, OKP cells transfected with eYFP-NaPi2c were treated with jasplakinolide, an agent that blocks microvillar treadmilling and locks the actin bundle (7). Transfected cells were imaged using apical TIR-FM. Jasplakinolide alone had no effect on the BB abundance of NaPi2c (Fig. 5, *B* and *D*). However, jasplakino-

lide blocked the PTH-induced removal of eYFP-NaPi2c from the BB membrane (Fig. 5, *C* and *D*), implying that a dynamic actin cytoskeleton is necessary for PTH-induced removal of NaPi2c from the BB.

Myosin VI is required for PTH-induced removal of NaPi2c from BB microvilli. To determine whether myosin VI is required for PTH-induced trafficking of NaPi2c from the proximal tubule BB, we used a dominant negative myosin VI motor mutant consisting of the tail domain of the protein without the motor domain. The myosin VI tail mutant is believed to act in a dominant negative manner to block myosin VI action by
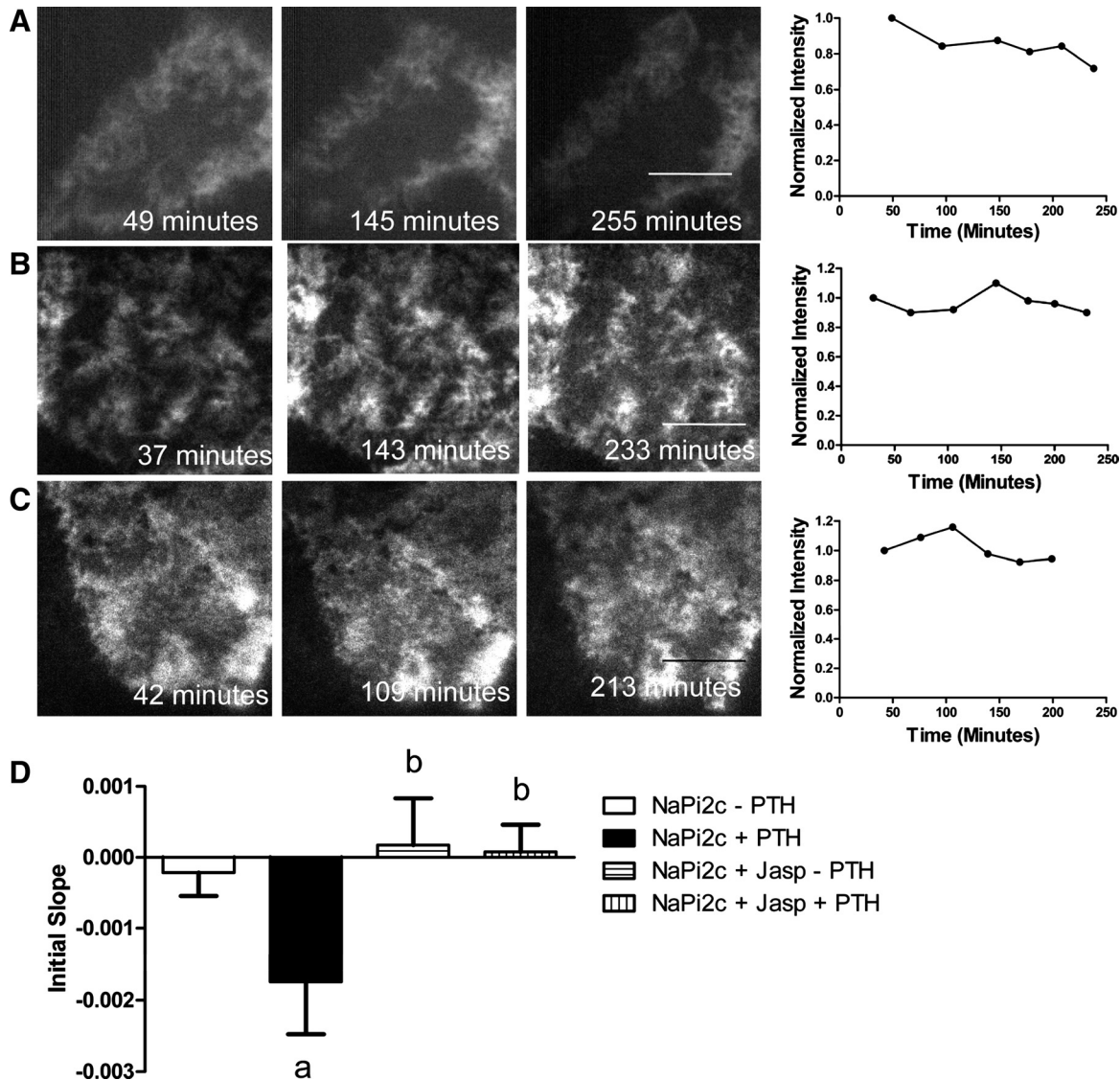

Fig. 5. A dynamic actin cytoskeleton is required for PTH-mediated removal of NaPi2c from the BBM. *A*: representative TIR-FM image of an OKP cell transfected with eYFP-NaPi2c and treated with PTH. The graph to the *right* of the images shows changes in fluorescence intensity over time. Fluorescence intensities were normalized to $t = 0$. Scale bars, 5 μm. *B*: representative TIR-FM image of an OKP cell transfected with eYFP-NaPi2c and treated with 1 μM jasplakinolide (an agent that locks the actin cytoskeleton) but not with PTH. The graph to the *right* of the images shows changes in fluorescence intensity over time. *C*: representative TIR-FM image of an OKP cell transfected with eYFP-NaPi2c and treated with jasplakinolide and PTH. The graph to the *right* of the images shows changes in fluorescence intensity over time. *D*: to compare changes in brush border fluorescence intensity over time across different cells, the slope of the intensity versus time graph for each cell was measured over the first 180 min (initial slope). A more negative slope indicates more rapid removal of NaPi2c from the BBM. The bar graphs represent the average initial slopes for OKP cells transfected with eYFP-NaPi2c and not treated with PTH (open bar, $n = 12$), treated with PTH (black bar, $n = 18$), treated with jasplakinolide (Jasp) but no PTH (horizontal hatched bar, $n = 4$), or treated with jasplakinolide and PTH (vertical hatched bar, $n = 10$). PTH treatment leads to a significant decrease in brush border fluorescence intensity of eYFP-NaPi2c over time ([a]$P < 0.05$ compared with NaPi2c − PTH). Jasplakinolide treatment blocks the PTH-induced decrease in BB fluorescence intensity of NaPi2c ([b]$P = $ NS compared with NaPi2c − PTH).

binding to cargo and preventing its movement (1). OKP cells were transfected with NaPi2c alone or cotransfected with eYFP-NaPi2c and CFP Myo6Tail and observed using apical TIR-FM. In the cotransfection experiments only cells that coexpressed both YFP- and CFP-tagged proteins were selected for study. We have previously shown using apical TIR-FM that the myosin VI tail mutant blocks PTH-induced removal of NaPi2a from the BBM (3).

Here we show the results of similar experiments using NaPi2c and the dominant negative myosin VI tail mutant. To control for any effects of cotransfecting the myosin VI dominant negative tail mutant into OKP cells, CFP-Myo6Tail was cotransfected with eYFP-NaPi2c into OKP cells and the cells were observed over time using apical TIR-FM. As can be seen in Fig. 6, B and D, there was no decrease in the BB abundance of NaPi2c in cells cotransfected with eYFP-NaPi2c and CFP-Myo6Tail and not treated with PTH. The average initial slope for OKP cells transfected with eYFP-NaPi2c and not treated with PTH was -0.0002 (SE 0.0003) compared with 0.00016 (SE 0.0006) for OKP cells cotransfected with eYFP-NaPi2c and CFP-Myo6Tail and not treated with PTH [P = not significant (NS) compared with NaPi2c alone $-$ PTH]. However, trafficking of eYFP-NaPi2c out of the BB in response to PTH was blocked in OKP cells cotransfected with eYFP-NaPi2c and CFP-Myo6Tail and treated with PTH (Fig. 6, C and D). The average initial slope for OKP cells cotransfected with eYFP-NaPi2c and CFP-Myo6Tail and treated with PTH was 0.0019

(SE 0.0004) compared with -0.0017 (SE 0.0007) for OKP cells transfected with eYFP-NaPi2c and treated with PTH ($P < 0.05$ for initial slope of NaPi2c + Myo6Tail + PTH compared with NaPi2c + PTH). This suggests that myosin VI is required for PTH-induced removal of NaPi2c from the proximal tubule BB.

The diffusion coefficient increases more rapidly for NaPi2a than NaPi2c after PTH treatment. Since myosin VI appears to be required for removal of both NaPi2a and NaPi2c from the BB in response to PTH, we investigated an alternate mechanism for the slower response of NaPi2c to PTH. We hypothesized that NaPi2c might be more tethered in the membrane than NaPi2a. We used FCS, a sensitive method for determining diffusion coefficients, to evaluate the diffusion coefficients of NaPi2a and NaPi2c in the apical cell membrane at baseline and after PTH (16, 32). OKP cells were transfected with GFP-tagged NaPi2a or mCherry-tagged NaPi2c, and FCS was performed in the presence or absence of PTH. At baseline there was no difference in the diffusion coefficients of NaPi2a and NaPi2c within the microvillar membrane (Fig. 7A). However, after addition of PTH there was a significant increase in the diffusion coefficient of NaPi2a at the apical membrane which occurred within 20 min of addition of PTH (Fig. 7B, left). A representative cell is shown in Fig. 7B, top. Results of four experiments are summarized in Fig. 7B, bottom. For NaPi2a, the average diffusion coefficient at time (t) = 0 to 10 min was 0.13 ± 0.02 $\mu m^2/s$, whereas at t = 11 to 20 min the average
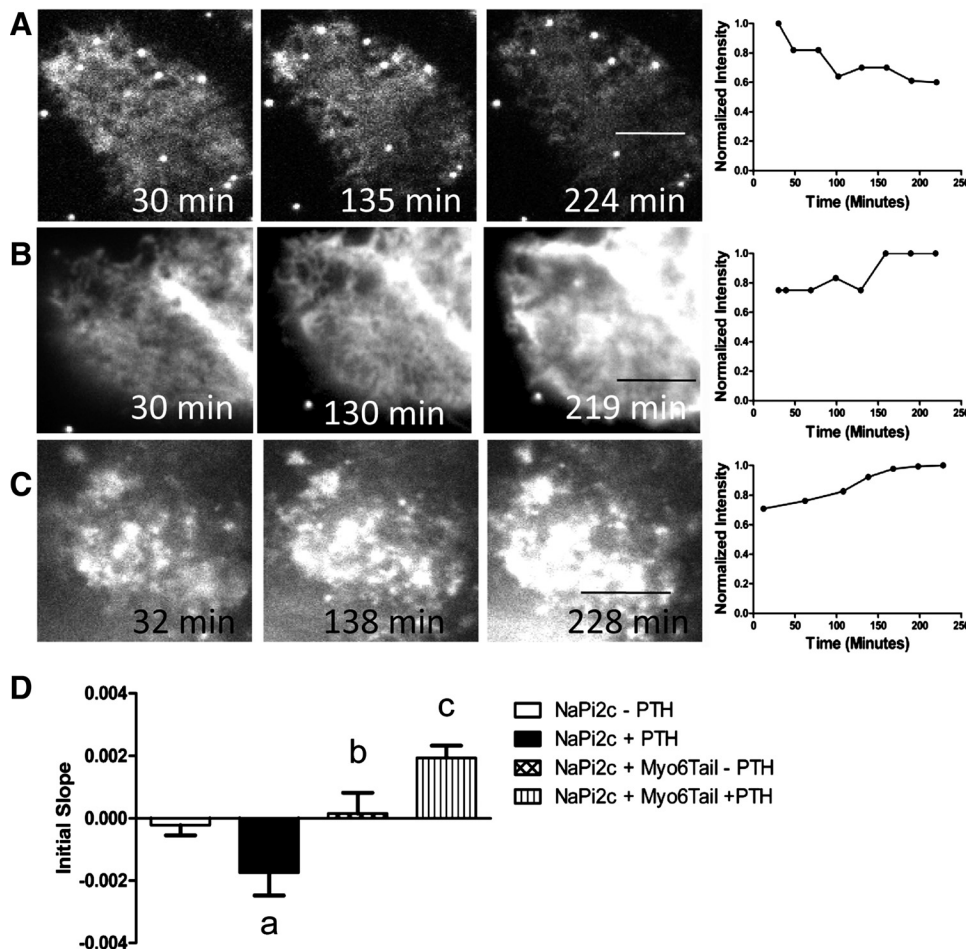
Fig. 6. Myosin VI is required for the removal of NaPi2c from the BBM in response to PTH. *A*: representative image and graph of fluorescence intensity versus time for OKP cell transfected with eYFP-NaPi2c and treated with PTH. *B*: representative image and graph of OKP cell cotransfected with eYFP-NaPi2c and CFP-Myo6Tail and not treated with PTH. *C*: representative image and graph of OKP cell cotransfected with eYFP-NaPi2c and CFP-Myo6Tail and treated with PTH. *D*: bar graphs represent the average initial slopes (measured over the first 180 min) for OKP cells transfected with eYFP-NaPi2c and not treated with PTH (open bar, n = 12), treated with PTH (black bar, n = 18), cotransfected with eYFP-NaPi2c and CFP-Myo6Tail and not treated with PTH (cross-hatched bar, n = 5), and cotransfected with eYFP-NaPi2c and CFP-Myo6Tail and treated with PTH (vertical hatched bar, n = 6). Cotransfection of the Myo6Tail mutant blocks removal of NaPi2c from the BBB in response to PTH ([a]$P <$ 0.05 compared with NaPi2a–PTH; [b]P = NS compared with NaPi2c–PTH; [c]$P <$ 0. 05 compared with NaPi2c + PTH). In certain panels (e.g., *A*), the fluorescent beads used in some cases to mark the bottom of the dish can be seen.
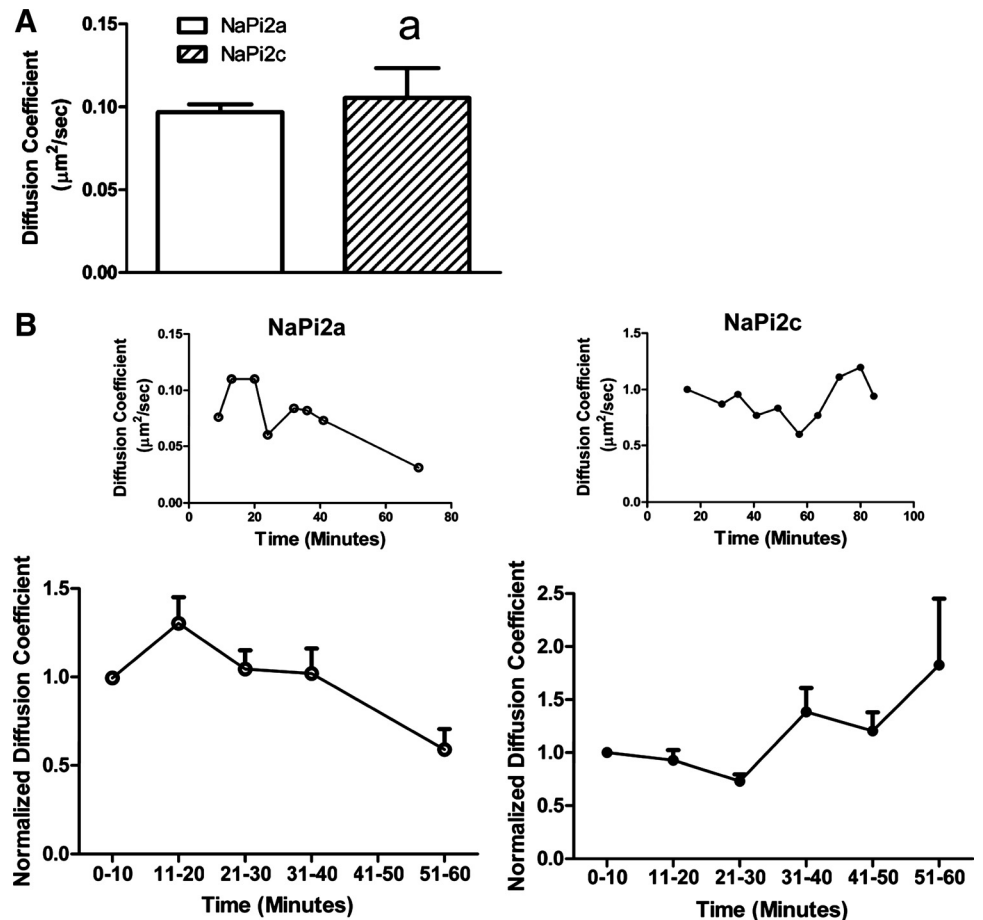
Fig. 7. NaPi2a shows an earlier increase in its diffusion coefficient in response to PTH compared with NaPi2c. OKP cells were transfected with either green fluorescent protein (GFP)-NaPi2a or mCherry NaPi2c. Diffusion coefficients of the cotransporters at the BBM were obtained using fluorescence correlation spectroscopy (FCS). *A*: at baseline there is no significant difference between the diffusion coefficient for NaPi2a (open bar, $n = 9$) versus NaPi2c (hatched bar, $n = 14$; [a]P = NS). *B*: smaller graphs (*top*) show a representative graph of the diffusion coefficients versus time for an OKP cell transfected with GFP-NaPi2a (○, *left*) or mCherry NaPi2c (●, *right*) and treated with 10^{-6} M PTH. The larger graphs (*bottom*) summarize the change in diffusion coefficients versus time for cells transfected with GFP-NaPi2a (○, *left*, $n = 5$) or mCherry NaPi2c (●, *right*, $n = 7$). To compare diffusion coefficients across experiments, for each cell, diffusion coefficients were normalized to that of the earliest time point obtained. After treatment with PTH, NaPi2a showed an early (within 20 min) increase in its diffusion coefficient, which was not seen for NaPi2c.

diffusion coefficient was 0.18 ± 0.01 μm^2/s ($P = 0.04$ compared with $t = 0$ to 10 min). This was not seen with NaPi2c (Fig. 7*B*, *right*). At $t = 0$ to 10 min, the average diffusion coefficient for NaPi2c was 0.14 ± 0.01 μm^2/s and at $t = 11$ to 20 min, the average diffusion coefficient was 0.13 ± 0.007 μm^2/s (P = NS compared with $t = 0$ to 10 min). This suggests that, after addition of PTH, NaPi2a is released from tethering structures (such as PDZ proteins) more rapidly than NaPi2c. This would account at least in part for the differential response of NaPi2a and NaPi2c to PTH.

To confirm the results obtained using FCS, we used another method to determine the diffusion coefficients of NaPi2a and NaPi2c within the BBM. We performed RICS on single microvilli using a SPT routine to keep the microvillus always at the center of a scanned circular orbit. During a tracking-RICS measurement, a microvillus, even if moving, appeared as stationary with respect to the scanned orbit. This prevented the measure of protein diffusion from being affected by the movement of the whole microvillus. Tracking-RICS measurements were performed on OKP cells cotransfected with Cerulean-tagged NaPi2a and mCherry-tagged NaPi2c allowing determination of diffusion coefficients for NaPi2a and NaPi2c within the same microvillus. In Fig. 8*A*, each graph represents a tracking-RICS curve for either NaPi2a (open circles) or NaPi2c (closed squares) within the same microvillus after treatment with PTH. For each pair of traces, the NaPi2a diffusion coefficient increases earlier than that of NaPi2c. The composite results

for the change in diffusion coefficients over time for NaPi2a (open circles, *left*) or NaPi2c (closed circles, *right*) are shown in Fig. 8*B*. As seen with FCS, after application of PTH, NaPi2a showed an early increase in its diffusion coefficient (within 15 min of PTH treatment), which was not seen for NaPi2c (compare Fig. 8*B*, *left* and *right*). For NaPi2a, the diffusion coefficient at $t = 0$ min was 0.08 ± 0.03 μm^2/s compared with 0.84 ± 0.36 μm^2/s at $t = 5$ min ($P < 0.05$ compared with $t = 0$) and 0.51 ± 0.43 μm^2/s at $t = 15$ min. For NaPi2c, the diffusion coefficient at $t = 0$ min was 0.18 ± 0.09 μm^2/s and at $t = 5$ min was 0.07 ± 0.02 μm^2/s (P = NS compared with $t = 0$). The diffusion coefficient at $t = 15$ min was 0.06 ± 0.01 μm^2/s (P = NS compared with $t = 0$).

DISCUSSION

Phosphorus homeostasis is crucial for normal cellular function, and the kidneys are critical regulators of phosphorus balance. The two predominant renal sodium phosphate cotransporters, NaPi2a and NaPi2c, are found in the brush border microvilli in renal proximal tubule cells (2, 23). Parathyroid hormone causes a decrease in the brush border abundance of the two cotransporters but with markedly different kinetics. NaPi2a is removed from the brush border within an hour of PTH application but the same process takes approximately four to six times longer for NaPi2c. Here we demonstrate that both NaPi2a and NaPi2c require a myosin motor, myosin VI, for
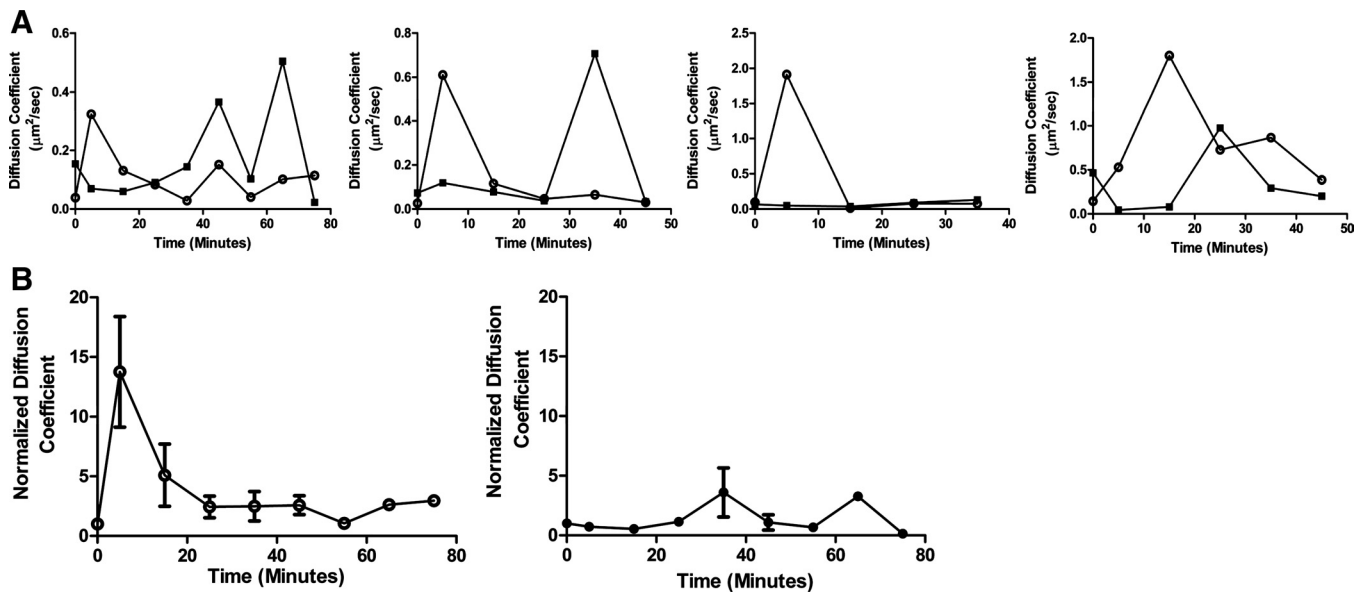
Fig. 8. Tracking RICS also demonstrates an earlier increase in the diffusion coefficient of NaPi2a compared with NaPi2c after treatment with PTH. OKP cells were cotransfected with Cerulean-NaPi2a and mCherry-NaPi2c and treated with 10^{-6} M PTH. *A*: each graph shows the change in diffusion coefficients over time in response to PTH for NaPi2a (○) versus NaPi2c (■) within the same microvillus. In each case NaPi2a shows an earlier increase in its diffusion coefficient than NaPi2c. *B*: to compare the change in diffusion coefficients after PTH treatment across experiments, diffusion coefficients were normalized to that at $t = 0$ min for each cell. Normalized diffusion coefficients versus time are plotted for NaPi2a (○, *left*, $n = 4$) or NaPi2c (●, *right*, $n = 4$).

PTH-induced removal of the cotransporters from the microvilli. NaPi2a, however, in response to PTH, shows a much earlier increase in its diffusion coefficient. This suggests that NaPi2a becomes untethered from membrane anchors much sooner than NaPi2c, which could partially explain the difference in the kinetic response to PTH. One caveat is that dynamic live cell imaging studies such as these are of necessity performed in vitro, and care should be taken when generalizing these findings.

A caveat to the observation that myosin VI acts to move NaPi2a or NaPi2c in the brush border microvilli in response to PTH is that, while these data were obtained using TIR-FM (which selectively illuminates events within 100 nm of the coverslip), the microvilli observed may have been lying on their sides. Every effort was made, however, to observe microvilli that appeared to be perpendicular to the coverslip. An additional caveat to these observations is that the effects of the myosin VI tail mutant may be secondary to effects of the mutant on myosin VI within the intervillar clefts or terminal web. It should be noted, however, that myosin VI has been shown to be present within brush border microvilli (41, 42).

It is interesting to note that, during the period that NaPi2c is still being removed from the BBM in response to PTH, the surface abundance of NaPi2a reached a nadir and then begins to increase (Fig. 1*A*). It is known that in response to PTH, NaPi2a is removed from the apical membrane and then sent to lysosomes for degradation (34). It has also been shown in OK cells that recovery of the surface abundance of NaPi2a after PTH treatment is dependent on de novo protein synthesis (33). Precisely which internal compartments NaPi2c is sent to after PTH treatment remains to be determined although the cotransporters are not believed to be directed to lysosomes (36).

Myosin VI has been shown to bind the adaptor proteins Disabled-2 (Dab2), the glucose-transporter binding protein (GIPC) (37), and, more recently, the adaptor AP-2 (9). The proteins that link the sodium phosphate cotransporters to myosin VI are unknown. Both NaPi2a and NaPi2c bind the adaptor proteins NHERF-1 and NHERF-3 (PDZK1) (22, 39). However, NaPi2a may bind NHERF-1 with much higher affinity than NaPi2c (14). It has been previously shown that NHERF-1 is required for PTH-induced signaling to NaPi2a via phospholipase C (8). If NHERF-1 is also required to mediate the PTH signal to NaPi2c, then one hypothesis to explain the more rapid removal of NaPi2a from the BBM in response to PTH is that the higher affinity of NaPi2a for NHERF-1 might allow its preferential removal from the apical membrane. This hypothesis requires further testing. Alternatively, PTH might signal to NaPi2c via PDZK1 but it might take an extended period of time for NaPi2c to become untethered from PDZK1 so that it can associate with myosin VI.

The lateral diffusion coefficients obtained for NaPi2a and NaPi2c within the brush border membrane are similar to those obtained for other membrane proteins in living cells (15, 29). At baseline the diffusion coefficients for both cotransporters are low, consistent with the notion that, within the membrane, the cotransporters are tethered by scaffolding proteins such as NHERF-1 and NHERF-3.

We used two different methods to demonstrate that, after PTH treatment, NaPi2a has an early increase in its diffusion coefficient that is not seen for NaPi2c. The advantage of the tracking-RICS method is that it allows analysis of the diffusion coefficients of NaPi2a and NaPi2c simultaneously within the same microvillus.

The finding of an early increase in the diffusion coefficient of NaPi2a after PTH treatment parallels that of Weinman et al.

(43), who found a nearly twofold increase in the percent mobile fraction of NaPi2a (measured by fluorescence recovery after photobleaching) within 10 min of PTH application. In their study a mutant NaPi2a lacking the ability to bind to NHERF-1 failed to show any increase in percent mobile fraction after addition of PTH, again suggesting the importance of this PDZ protein in mediating PTH-induced removal of NaPi2a from the BBM.

The events governing binding and unbinding of microvillar PDZ proteins to the sodium phosphate cotransporters in response to PTH remain to be determined. In the case of the NaPi2a/NHERF-1 complex, PTH induces phosphorylation of NHERF-1, which promotes dissociation of the NaPi2a/NHERF-1 complex (42). Little is known about phosphorylation events or conformational changes of NaPi2c/PDZ protein complexes in response to PTH.

In summary, we have shown that, while the time course of removal of NaPi2a and NaPi2c from the brush border membrane in response to PTH is very different, both cotransporters require myosin VI for PTH-induced trafficking in microvilli. In response to PTH, however, the diffusion coefficient of NaPi2a within the BBM increases early, whereas that of NaPi2c does not, implying that the two cotransporters are released from membrane tethers on different timescales. Further work is needed to identify which NaPi2a or NaPi2c PDZ protein interactions are important for linking the cotransporters to myosin VI in response to PTH.

DISCLOSURES

No conflicts of interest, financial or otherwise, are declared by the author(s).

REFERENCES

1. **Aschenbrenner L, Lee T, Hasson T.** Myo6 facilitates the translocation of endocytic vesicles from cell peripheries. *Mol Biol Cell* 14: 2728–2743, 2003.
2. **Biber J, Hernando N, Forster I, Murer H.** Regulation of phosphate transport in proximal tubules. *Pflügers Arch* 458: 39–52, 2009.
3. **Blaine J, Okamura K, Giral H, Breusegem S, Caldas Y, Millard A, Barry N, Levi M.** PTH-induced internalization of apical membrane NaPi2a: role of actin and myosin VI. *Am J Physiol Cell Physiol* 297: C1339–C1346, 2009.
4. **Bretscher A, Weber K.** Localization of actin and microfilament-associated proteins in the microvilli and terminal web of the intestinal brush border by immunofluorescence microscopy. *J Cell Biol* 79: 839–845, 1978.
5. **Breusegem SY, Takahashi H, Giral-Arnal H, Wang X, Jiang T, Verlander JW, Wilson P, Miyazaki-Anzai S, Sutherland E, Caldas Y, Blaine JT, Segawa H, Miyamoto Ki Barry NP, Levi M.** Differential regulation of the renal sodium-phosphate cotransporters NaPi-IIa, NaPi-IIc, and PiT-2 in dietary potassium deficiency. *Am J Physiol Renal Physiol* 297: F350–F361, 2009.
6. **Brown JW, McKnight CJ.** Molecular model of the microvillar cytoskeleton and organization of the brush border. *PLoS One* 5: e9406, 2010.
7. **Bubb MR, Senderowicz AM, Sausville EA, Duncan KL, Korn ED.** Jasplakinolide, a cytotoxic natural product, induces actin polymerization and competitively inhibits the binding of phalloidin to F-actin. *J Biol Chem* 269: 14869–14871, 1994.
8. **Capuano P, Bacic D, Roos M, Gisler SM, Stange G, Biber J, Kaissling B, Weinman EJ, Shenolikar S, Wagner CA, Murer H.** Defective coupling of apical PTH receptors to phospholipase C prevents internalization of the Na$^+$-phosphate cotransporter NaPi-IIa in Nherf1-deficient mice. *Am J Physiol Cell Physiol* 292: C927–C934, 2007.
9. **Collaco A, Jakab R, Hegan P, Mooseker M, Ameen N.** Alpha-AP-2 directs myosin VI-dependent endocytosis of cystic fibrosis transmembrane conductance regulator chloride channels in the intestine. *J Biol Chem* 285: 17177–17187, 2010.
10. **Deliot N, Hernando N, Horst-Liu Z, Gisler SM, Capuano P, Wagner CA, Bacic D, O'Brien S, Biber J, Murer H.** Parathyroid hormone treatment induces dissociation of type IIa Na$^+$-Pi cotransporter-Na$^+$/H$^+$ exchanger regulatory factor-1 complexes. *Am J Physiol Cell Physiol* 289: C159–C167, 2005.
11. **Digman MA, Brown CM, Sengupta P, Wiseman PW, Horwitz AR, Gratton E.** Measuring fast dynamics in solutions and cells with a laser scanning microscope. *Biophys J* 89: 1317–1327, 2005.
12. **Digman MA, Sengupta P, Wiseman PW, Brown CM, Horwitz AR, Gratton E.** Fluctuation correlation spectroscopy with a laser-scanning microscope: exploiting the hidden time structure. *Biophys J* 88: L33–L36, 2005.
13. **Forster IC, Hernando N, Biber J, Murer H.** Proximal tubular handling of phosphate: a molecular perspective. *Kidney Int* 70: 1548–1559, 2006.
14. **Giral H, Lanzano L, Caldas Y, Blaine J, Verlander JW, Lei T, Gratton E, Levi M.** Role of PDZ domain containing 1 (PDZK1) in apical membrane expression of renal Na-coupled phosphate (Na/Pi) transporters. *J Biol Chem* 286: 15032–15042, 2011.
15. **Hegener O, Prenner L, Runkel F, Baader SL, Kappler J, Häberlein H.** Dynamics of beta2-adrenergic receptor-ligand complexes on living cells. *Biochemistry* 43: 6190–6199, 2004.
16. **Kim SA, Heinze KG, Schwille P.** Fluorescence correlation spectroscopy in living cells. *Nat Methods* 4: 963–973, 2007.
17. **Koyama HGC, Miller MM, Teplitz RL, Riggs AD.** Establishment and characterization of a cell line from the American opossum (*Didelphys virginiana*). *In Vitro* 14: 239–246, 1978.
18. **LaLonde DP, Garbett D, Bretscher A.** A regulated complex of the scaffolding proteins PDZK1 and EBP50 with ezrin contribute to microvillar organization. *Mol Biol Cell* 21: 1519–1529, 2010.
19. **Lanzano L, Digman MA, Fwu P, Giral H, Levi M, Gratton E.** Nanometer-scale imaging by the modulation tracking method. *J Biophotonics* 4: 415–424, 2011.
20. **Lederer ED, Khundmiri SJ, Weinman EJ.** Role of NHERF-1 in regulation of the activity of Na-K ATPase and sodium-phosphate co-transport in epithelial cells. *J Am Soc Nephrol* 14: 1711–1719, 2003.
21. **Lederer ED, Sohi SS, Mathiesen JM, Klein JB.** Regulation of expression of type II sodium-phosphate cotransporters by protein kinases A and C. *Am J Physiol Renal Physiol* 275: F270–F277, 1998.
22. **Levi M, Blaine J, Breusegem S, Takahashi H, Sorribas V, Barry N.** Renal phosphate-wasting disorders. *Adv Chronic Kidney Dis* 13: 155–165, 2006.
23. **Levi M, Bruesegem S.** Renal phosphate-transporter regulatory proteins and nephrolithiasis. *N Engl J Med* 359: 1171–1173, 2008.
24. **Levi V, Ruan Q, Gratton E.** 3-D particle tracking in a two-photon microscope: application to the study of molecular dynamics in cells. *Biophys J* 88: 2919–2928, 2005.
25. **Levi V, Ruan Q, Plutz M, Belmont AS, Gratton E.** Chromatin dynamics in interphase cells revealed by tracking in a two-photon excitation microscope. *Biophys J* 89: 4275–4285, 2005.
26. **Lotscher M, Scarpetta Y, Levi M, Halaihel N, Wang H, Zajicek HK, Biber J, Murer H, Kaissling B.** Rapid downregulation of rat renal Na/Pi cotransporter in response to parathyroid hormone involves microtubule rearrangement. *J Clin Invest* 104: 483–494, 1998.
27. **Madjdpour C, Bacic D, Kaissling B, Murer H, Biber J.** Segment-specific expression of sodium-phosphate cotransporters NaPi-IIa and -IIc and interacting proteins in mouse renal proximal tubules. *Pflügers Arch* 448: 402–410, 2004.
28. **Mahon MJ, Segre GV.** Stimulation by parathyroid hormone of a NHERF-1-assembled complex consisting of the parathyroid hormone I receptor, phospholipase Cbeta, and actin increases intracellular calcium in opossum kidney cells. *J Biol Chem* 279: 23550–23558, 2004.
29. **Meissner O, Häberlein H.** Lateral mobility and specific binding to GABAA receptors on hippocampal neurons monitored by fluorescence correlation spectroscopy. *Biochemistry* 42: 1667–1672, 2003.
30. **Miyamoto Ki Segawa H, Ito M, Kuwahata M.** Physiological regulation of renal sodium-dependent phosphate cotransporters. *Jpn J Physiol* 54: 93–102, 2004.

31. **Murer H, Hernando N, Forster I, Biber J.** Regulation of Na/Pi transporter in the proximal tubule. *Annu Rev Physiol* 65: 531–542, 2003.

32. **Petrásek Z, Schwille P.** Precise measurement of diffusion coefficients using scanning fluorescence correlation spectroscopy. *Biophys J* 94: 1437–1448, 2008.

33. **Pfister MF, Lederer E, Forgo J, Ziegler U, Lotscher M, Quabius ES, Biber J, Murer H.** Parathyroid hormone-dependent degradation of type II Na$^+$/Pi cotransporters. *J Biol Chem* 272: 20125–20130, 1997.

34. **Pfister MF, Ruf I, Stange G, Ziegler U, Lederer E, Biber Jr, Murer H.** Parathyroid hormone leads to the lysosomal degradation of the renal type II Na/Pi cotransporter. *Proc Natl Acad Sci USA* 95: 1909–1914, 1998.

35. **Rzadzinska AK, Schneider ME, Davies C, Riordan GP, Kachar B.** An actin molecular treadmill and myosins maintain stereocilia functional architecture and self-renewal. *J Cell Biol* 164: 887–897, 2004.

36. **Segawa H, Yamanaka S, Onitsuka A, Tomoe Y, Kuwahata M, Ito M, Taketani Y, Miyamoto Ki.** Parathyroid hormone-dependent endocytosis of renal type IIc Na-Pi cotransporter. *Am J Physiol Renal Physiol* 292: F395–F403, 2007.

37. **Spudich G, Chibalina MV, Au JSY, Arden SD, Buss F, Kendrick-Jones J.** Myosin VI targeting to clathrin-coated structures and dimerization is mediated by binding to Disabled-2 and PtdIns(4,5)P2. *Nat Cell Biol* 9: 176–183, 2007.

38. **Tyska MJ, Mooseker MS.** MYO1A (brush border myosin I) dynamics in the brush border of LLC-PK1-CL4 cells. *Biophys J* 82: 1869–1883, 2002.

39. **Villa-Bellosta R, Barac-Nieto M, Breusegem SY, Barry NP, Levi M, Sorribas V.** Interactions of the growth-related, type IIc renal sodium/phosphate cotransporter with PDZ proteins. *Kidney Int* 73: 456–464, 2007.

40. **Villa-Bellosta R, Ravera S, Sorribas V, Stange G, Levi M, Murer H, Biber J, Forster IC.** The Na$^+$-Pi cotransporter PiT-2 (SLC20A2) is expressed in the apical membrane of rat renal proximal tubules and regulated by dietary Pi. *Am J Physiol Renal Physiol* 296: F691–F699, 2009.

41. **Villa-Bellosta R, Sorribas V.** Compensatory regulation of the sodium/phosphate cotransporters NaPi-IIc (SCL34A3) and Pit-2 (SLC20A2) during Pi deprivation and acidosis. *Pflügers Arch* 459: 499–508, 2010.

42. **Weinman EJ, Biswas RS, Peng Q, Shen L, Turner CL, EX, Steplock D, Shenolikar S, Cunningham R.** Parathyroid hormone inhibits renal phosphate transport by phosphorylation of serine 77 of sodium-hydrogen exchanger regulatory factor-1. *J Clin Invest* 117: 3412–3420, 2007.

43. **Weinman EJ, Steplock D, Cha B, Kovbasnjuk O, Frost NA, Cunningham R, Shenolikar S, Blanpied TA, Donowitz M.** PTH transiently increases the percent mobile fraction of Npt2a in OK cells as determined by FRAP. *Am J Physiol Renal Physiol* 297: F1560–F1565, 2009.

44. **Yang LE, Leong PKK, McDonough AA.** Reducing blood pressure in SHR with enalapril provokes redistribution of NHE3, NaPi2, and NCC and decreases NaPi2 and ACE abundance. *Am J Physiol Renal Physiol* 293: F1197–F1208, 2007.

45. **Yang LE, Maunsbach AB, Leong PKK, McDonough AA.** Redistribution of myosin VI from top to base of proximal tubule microvilli during acute hypertension. *J Am Soc Nephrol* 16: 2890–2896, 2005.